



## Model reduction for the forming process of fibrous composites structures via second gradient enriched continuum models

Gabriele Barbagallo, Marco Valerio d'Agostino, Alexios Aivaliotis, Ali Daouadji, Ahmed Makradi, Gaetano Giunta, Philippe Boisse, Salim Belouettar & Angela Madeo

To cite this article: Gabriele Barbagallo, Marco Valerio d'Agostino, Alexios Aivaliotis, Ali Daouadji, Ahmed Makradi, Gaetano Giunta, Philippe Boisse, Salim Belouettar & Angela Madeo (2019): Model reduction for the forming process of fibrous composites structures via second gradient enriched continuum models, *Mechanics of Advanced Materials and Structures*, DOI: [10.1080/15376494.2019.1629050](https://doi.org/10.1080/15376494.2019.1629050)

To link to this article: <https://doi.org/10.1080/15376494.2019.1629050>



© 2019 The Author(s). Published with license by Taylor & Francis Group, LLC.



Published online: 12 Sep 2019.



Submit your article to this journal [↗](#)



Article views: 543



View related articles [↗](#)



View Crossmark data [↗](#)

# Model reduction for the forming process of fibrous composites structures via second gradient enriched continuum models

Gabriele Barbagallo<sup>a</sup> , Marco Valerio d'Agostino<sup>a</sup> , Alexios Aivaliotis<sup>a</sup>, Ali Daouadji<sup>a</sup> , Ahmed Makradi<sup>b</sup> , Gaetano Giunta<sup>b</sup> , Philippe Boisse<sup>a</sup> , Salim Belouettar<sup>b</sup> , and Angela Madeo<sup>a</sup> 

<sup>a</sup>INSA-Lyon, Université de Lyon, Villeurbanne cedex, France; <sup>b</sup>Luxembourg Institute of Science and Technology, Esch-sur-Alzette, Luxembourg

## ABSTRACT

This paper describes phenomena associated to the microstructure, such as the local bending stiffness of the yarns, with a second gradient parameter associated to terms in the energy with higher order derivatives. The results obtained with this enriched continuous model are presented and it is shown how the main deformation mode can be controlled to reproduce experimental evidence. In particular, increasing the second gradient parameter, the deformation mode switches from shear to one with a constant curvature along the specimen. Two fibrous composite reinforcements with two different geometries are modeled: composite airframe for aeronautic industry and an automotive leaf-spring for automotive industry. The two application cases are described as homogeneous second gradient continua with an energy depending on the in-plane and out-of-plane curvature of the yarns. This addition allows to take into account the effects of the local bending stiffness of the yarns at the mesoscale in a homogenized way.

## ARTICLE HISTORY

Received 19 April 2019  
Accepted 1 June 2019



## KEYWORDS

Model reduction; enriched continuum models; forming process; fibrous composites; decision making; material and process selection

## 1. Introduction

Modeling and simulation of composite material and structures and related manufacturing processes could reduce drastically the resources needed to improve/reinvent the production chain. To obtain this admittedly optimistic goal, we need to develop and integrate models for the reliable prediction of material behavior at different scales, as well as deriving efficient material-processing-property relationships. The current material selection processes (MSPs) in the field of composites (and, thus, composites structural design) don't usually include material models, while relying on experience and/or empirical methods. The reasons for this shortcoming of the industry are several, the increased complexity of the products, the global economic competition pressuring the industry to give short term results, the investments needed initially for R&D and much more. However, modeling and simulation for MSP and production could give a boost to efficiency and revenue through shorter lead-time, better product quality, more competitive cost, and higher customer satisfaction. A key-point of such MSP process is the integration of material models that account for a wide set of materials and structures performance indicators such stiffness, failure or instability. Developments and improvements have been taking place for different types of models and phenomena on several different length scales, with advancements in the so-called multiscale approaches, multi-disciplinary design optimization, and visualization. Important links within a hierarchy of processing, nano/

microstructure properties, and expected performance are currently available. Nevertheless, they are far from being sufficient for materials design and selection, and suffer from a lack of integration across different types of models and related communities (especially discrete/continuum and modeling/experimental coupling and validation). In this perspective and for complex structural materials, there is a particular need in industry for chemistry/physics-based material models and modeling workflows for the MSP that fulfill the following requirements: (i) prediction of relevant properties and key performance indicators (KPIs) that capture the performance of materials and finished pieces, accounting for the internal microstructure and effects of processing [1] and (ii) accuracy/validation of predicted data and relevant management of uncertainty [2]. To be reliable, such decision-making process must be built upon physical and engineering frameworks and based on methods that are systematic, effective and efficient in modeling complex, hierarchical materials. For material design and selection, understanding and quantifying the links between material structure at the nano- and micro-scale and their macroscopic effects is, therefore, essential (e.g. see [3]). Moreover, having macroscopic models that can effectively describe the all the micro-structure related phenomenon is of paramount importance. However, the complexity of the analyzed materials combined with the lack of a continued and solid connection between industry and academia tends to prevent the adoption and usage of innovative models that better

**CONTACT** Salim Belouettar  salim.belouettar@list.lu  Luxembourg Institute of Science and Technology, Esch-sur-Alzette, 4362 Luxembourg. Color versions of one or more of the figures in the article can be found online at [www.tandfonline.com/umcm](http://www.tandfonline.com/umcm).

This article has been republished with minor changes. These changes do not impact the academic content of the article.

© 2019 The Author(s). Published with license by Taylor & Francis Group, LLC.

This is an Open Access article distributed under the terms of the Creative Commons Attribution-NonCommercial-NoDerivatives License (<http://creativecommons.org/licenses/by-nc-nd/4.0/>), which permits non-commercial re-use, distribution, and reproduction in any medium, provided the original work is properly cited, and is not altered, transformed, or built upon in any way.

describe the thermo-mechanical/chemical behavior of complex materials. A clearcut example of materials whose conventional models fail to thoroughly describe the macroscopic characteristic of microstructured materials are the dry fibrous composite reinforcements (i.e. without resin). To model the preforming of woven composites, the most widespread macroscopic mechanical models are based on classical Cauchy continuum mechanics. Such models account accurately only for the deformation modes that can be effectively measured via the first derivatives of the displacement, so neglecting additional behavior related, for example, to the bending of yarns and fibers, see [4, 5]. On the other hand, enriched continuum theories can account for the mechanical properties of yarns and fibers in a homogenized matter, including the macroscopic effects of local phenomena. For this reason, our approach has been to implement a second gradient material that describes the energy related to micro-structural properties such as the bending of the fibers. In previous contributions, second gradient models have already been proposed and validated to describe the mechanical behavior of fibrous composite reinforcements (see [6–11]). In particular in [8], it was proven how the insertion of a second gradient energy can control the onset and evolution of wrinkling during the deep-drawing simulation, while increasing the numerical stability of the simulation.

The aim of this paper is to present additional properties of this model, while framing it inside modeling workflows for MSPs of fibrous composite reinforcements. The second gradient model is implemented in COMSOL® looking for solutions that are continuous, as it is usual in FEM, but that also grant continuity of the first derivatives of the displacement field. The effects of the second gradient on the results and to propose how to best choose the parameters to describe the properties of the resulting composite is demonstrated. The preliminary results obtained for case studies pertaining to the two aeronautical/automotive application cases is presented.

## 2. Second gradient modeling of 3D fibrous composite reinforcements

We define the Lagrangian configuration  $B_L \subset \mathbb{R}^3$  and the kinematical field  $\chi(X, t)$  which links to any material point  $X \in B_L$  its present position  $x$  at time  $t$ , so describing the deformation of the continuum. Since they will be used in the following, we also introduce the displacement field  $u(X, t) := \chi(X, t) - X$ , the tensor  $F := \nabla \chi$  and the Right Cauchy-Green deformation tensor  $C$ . Furthermore, the directions  $D_1$  and  $D_2$  indicate the direction of the warp and weft yarns in the Lagrangian configuration and  $D_3 = D_1 \times D_2$  indicates the normal to the plane containing them. Finally, the first gradient kinematics of the continuum must be complemented via a second order tensor field  $\nabla C$  which includes the microstructural effects in a homogenized way. The strain energy density  $W(C, \nabla C)$  implemented in this paper will assume a decomposition of the form:

$$W(C, \nabla C) = W_I(C) + W_{II}(\nabla C) \quad (1)$$

In the next subsections, we will define the first and second gradient energies  $W_I(C)$  and  $W_{II}(\nabla C)$  and present the associated constitutive parameters.

### 2.1. Hyperelastic first gradient model

In the literature, isotropic strain energies for the behavior of isotropic materials are available even at finite strains (see e.g. [12, 13]). On the other hand, strain energies are harder to find for orthotropic materials. Some examples are given in [14], where some polyconvex energies are proposed for rubbers in uniaxial tests. Other cases of polyconvex energies for anisotropic solids are available in [15]. Despite the studies of polyconvexity, which surely present a thorough basis for the investigation of hyperelastic materials, their use is frequently limited by the unclear attribution of physical meaning to the constitutive parameters which are included in the model. The approach embraced here is to introduce the minimum conceivable number of physically sensible constitutive parameters which are expected to capture the analyzed behavior.

In this subsection, we will present the constitutive equation for the first gradient strain energy density  $W_I(C)$ , which will be used to describe the fibrous composite reinforcement. A first gradient orthotropic energy can be completely defined with an expression of the kind (see e.g. [16] and the A where a theorem for the complete representation is presented):

$$W_I(C) = W_I(i_{11}, i_{22}, i_{33}, i_{12}, i_{13}, i_{23}), \quad (2)$$

where  $i_{ii} = D_i \cdot C \cdot D_i$ ,  $i = \{1, 2, 3\}$  are the elongation strains in the direction  $D_i$  and  $i_{ij} = D_i \cdot C \cdot D_j$  are shear strains between the directions  $D_i$  and  $D_j$  with  $i, j \in \{1, 2, 3\}$  and  $i \neq j$ .

We could define complex non-linear energies that catch every mechanical non-linearity of the experimental evidences, as done in [5, 17, 18], however this isn't one of the goals of the present work. Rather, using a straightforward quadratic first gradient energy, we can study the impact of the extra second gradient terms on the performed numerical simulations. Therefore, the chosen constitutive expression for the first gradient energy is:

$$W_I(C) = \frac{1}{2}K_{11}(\sqrt{i_{11}}-1)^2 + \frac{1}{2}K_{22}(\sqrt{i_{22}}-1)^2 + \frac{1}{2}K_{33}(\sqrt{i_{33}}-1)^2 + \frac{1}{2}K_{12}i_{12}^2 + \frac{1}{2}K_{13}i_{13}^2 + \frac{1}{2}K_{23}i_{23}^2, \quad (3)$$

where  $K_{ii}$  are the extensional stiffnesses of the material in the direction of the yarns and in the orthogonal direction, while  $K_{ij}$  with  $i \neq j$  are the in-plane and out-of plane shear stiffnesses. Woven composite reinforcements are materials in which the extensional stiffness is significantly higher than the shear one, and the in-plane shear stiffness is bigger than the out-of-plane one. In addition, the extensional stiffness in the normal plane is much lower than the in-plane ones, because no yarns woven through the thickness of the interlock. Regardless of whether more refined hyperelastic laws could be presented as in [5, 17, 18], the proposed expression for the first gradient energy density reflects the fundamental deformation modes of fibrous interlocks. For the choice of the parameters, the same principles assumed in [8] were followed and therefore the same values were chosen, see

**Table 1.** The only difference is the value of the out-of-plane shear rigidities in the first application case that, given the limited thickness and the absence of weaving on the third direction, was increased to 50 kPa.

## 2.2. Hyperelastic orthotropic second gradient strain energy density

Considering woven fabrics, the fundamental micro-structure-related deformation mechanism is the bending stiffness of the yarns that occurs at the mesoscopic level. The bending stiffness of the yarns is crucial for the reproduction of some particular effects, such as shear transition layers in 2D experimental tests and wrinkling during the deep-drawing of dry woven fabrics. Therefore, we will only introduce second energy terms that describe the consequent effects. A second gradient theory would be rich enough to account for other micro-structural related phenomena, but being not pivotal for the material analyzed they will not be included.

The second gradient energy considered is, accordingly, defined on the derivatives of the invariants  $i_{ij}$  ( $i \neq j$ ), accounting approximately for the curvatures of the two sets of yarns of the fabric. Given the family of yarns in the direction  $D_1$ ,  $i_{12,1}$  can be considered to be a measure of their in-plane bending<sup>1</sup> (see also [7, 9–11]). Similarly,  $i_{12,2}$  describes the in-plane bending of the other set of yarns. On the other hand,  $i_{13,1}$  and  $i_{23,2}$  account for the out-of-plane bending of the first and second set of yarns, respectively. The quantities  $i_{13,3}$  and  $i_{23,3}$  are not included here since we assume that there are no yarns in the out-of-plane direction. Due to these considerations, the second gradient strain energy density is of the form:

$$W_{II}(\nabla C) = \frac{1}{2} \alpha_1 i_{12,1}^2 + \frac{1}{2} \alpha_2 i_{12,2}^2 + \frac{1}{2} \beta_1 i_{13,1}^2 + \frac{1}{2} \beta_2 i_{23,2}^2, \quad (4)$$

where  $\alpha_1$ ,  $\alpha_2$  and  $\beta_1$ ,  $\beta_2$  are the in-plane and out-of-plane bending stiffnesses of the two families of yarns, respectively. In the rest of the paper, we will consider the in-plane and out-of-plane bending stiffnesses of the two families of yarns to be equal ( $\alpha = \alpha_1 = \alpha_2 = \beta_1 = \beta_2$ ), i.e.:

$$W_{II}(\nabla C) = \frac{1}{2} \alpha \left( i_{12,1}^2 + i_{12,2}^2 + i_{13,1}^2 + i_{23,2}^2 \right). \quad (5)$$

Additional work is needed to define a connection between the microstructure and the energy presented: the second gradient parameters must be related to a characteristic length  $L_c$  which depends on the scale of the microstructure of the material. Numerous identification strategies have been proposed to link the macroscopic second gradient parameter to the microscopic properties, e.g. see [19–21]. Therefore, some multi-scale methods may be applied in the future to case of woven composite reinforcements.

In the simulations, we will consider the tentative values  $\alpha = 0, 1, 10, 100$  [N]. If we consider a relation of the type

**Table 1.** Parameters of the first gradient energy.

$K_{11}$	$K_{22}$	$K_{33}$	$K_{12}$	$K_{13}^{\text{Case 1}}$	$K_{23}^{\text{Case 1}}$	$K_{13}^{\text{Case 2}}$	$K_{23}^{\text{Case 2}}$
5 MPa	5 MPa	0.5 MPa	50 kPa	50 kPa	50 kPa	0.5 kPa	0.5 kPa

$\alpha = K_{12} L_c^2$ , we can have an estimate of the resulting characteristic lengths  $L_c \simeq 0, 4, 14, 45$  [mm].<sup>2</sup> These values, in particular the last one, are very high but they are chosen to clearly show the effects of their introduction.

## 2.3. Augmented continuity shape functions

In the finite element method, the solution of the problem is searched among a subset of functions approximating the space of configurations. As explained in [22], it is implicitly assumed in the derivation of the equations in the finite element model that no contribution to the virtual work arises at element interfaces. Therefore, it is necessary to choose displacement functions such that the strains at the interface between elements are finite (even though they may be discontinuous). In the first gradient models, the strain is defined by first derivatives and, therefore, the displacements only have to be continuous. If, however, the strains depend on the second derivatives, as in the second gradient model, the continuity of the first derivatives must also be granted.

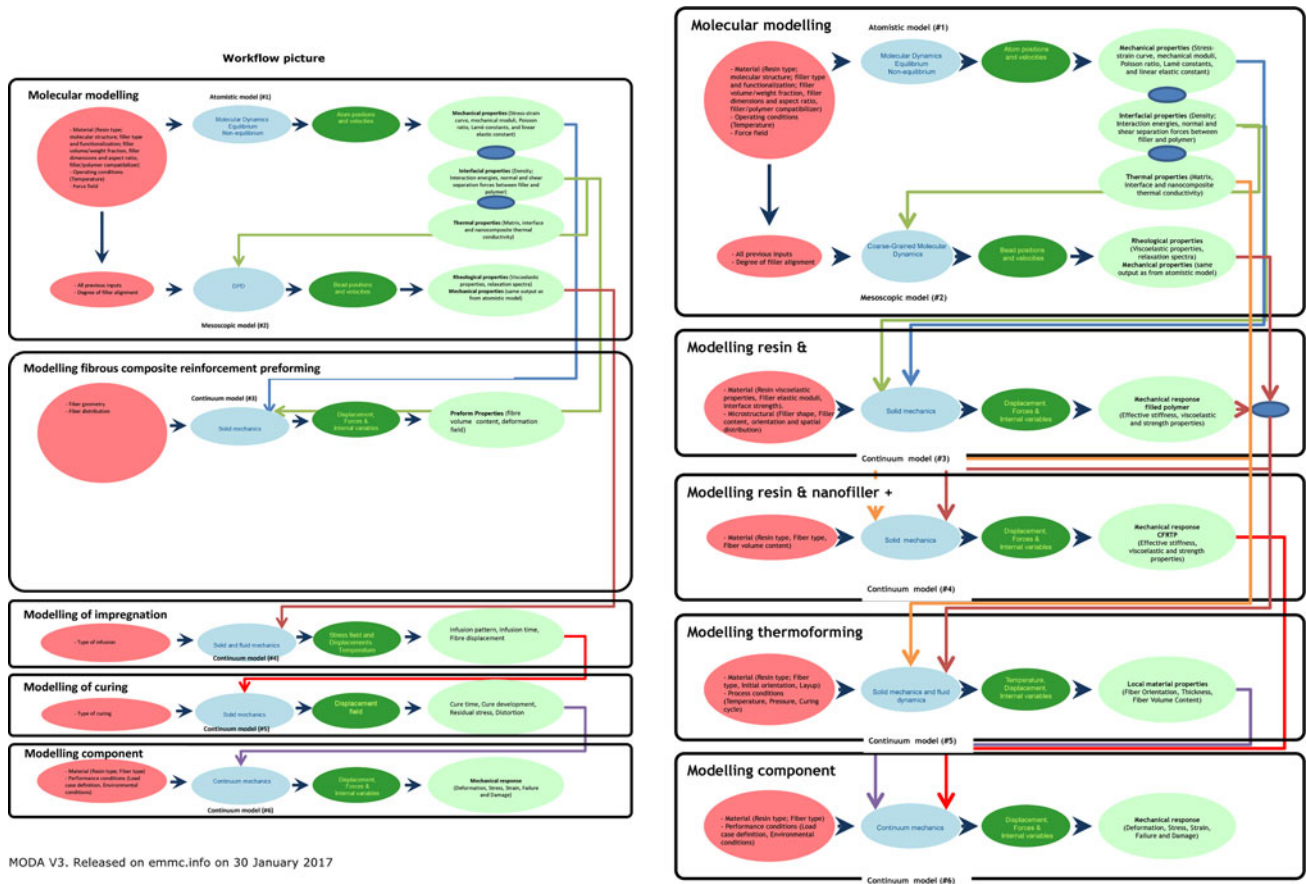
Therefore, it is important to choose one class of shape functions fit for the analysis of a second gradient model. In the one dimensional case, there would be various possible choices to be made. For instance, the Hermitian polynomials were born to evaluate problems such as the beam, in which the second derivatives of the displacement (the curvature of the beam in particular) play an important role. A different possibility are the Spline functions which guarantee a higher level of continuity (class  $C^{n-1}$  for polynomials of degree  $n$ ) between elements and would therefore be fit for this application.

In the case of 2D and 3D solids the problem becomes even more complicated: instead of having to consider one derivative we have to face the full gradient of the displacements  $\nabla u$ . As a matter of fact, the 2D and 3D Hermite functions have continuous derivatives between mesh elements, but only at the mesh vertices. In the 2D case, the Argyris functions (5th order polynomials) or B-splines would assure the continuity in the entire edge of the element (for the use of B-Splines in high continuity 2D problems see for example [23, 24]). Considering the complete 3D case, the only existing compatible elements ( $C^1$  continuity) are of at least 9th order [25] based on the Ženišek element [26]. Unfortunately those kind of elements imply such a high order of polynomials that are not currently implemented in the most widespread finite element softwares.

However, the need for continuity is due to the absence of contribution to the virtual work at element interfaces. As done in [8], we chose to implement third order Lagrangian polynomials with *augmented continuity* adding an a posteriori penalty energy related to the discontinuity of the

<sup>1</sup>Here and in the sequel, the term  $(\cdot)_j$  indicates the partial derivative of the quantity  $(\cdot)$  with respect to the variable  $\xi_j$  of a reference frame oriented along the directions  $D_j$ .

<sup>2</sup>On the other hand, if we considered a relation of the type  $\alpha = K_{11} L_c^2$ , we would have a much lower estimation of the resulting characteristic lengths  $L_c \simeq 0, 0.04, 0.14, 0.45$  [mm].



MODA V3. Released on emmc.info on 30 January 2017

Figure 1. Modeling Data (MODA) for the Leaf spring and Airframe application case.

deformations  $i_{12}$ ,  $i_{13}$ , and  $i_{23}$  at the element interfaces of the type<sup>3</sup>:

$$W_{\text{Interface}} = K_{\text{Penalty}} \left( [[i_{12}]]^2 + [[i_{13}]]^2 + [[i_{23}]]^2 \right). \quad (6)$$

This energy depends only on the discontinuity of the in-plane and out-of-plane shear deformations  $i_{12}$ ,  $i_{13}$ , and  $i_{23}$  and it is, therefore, not sufficient to render the entire  $\nabla u$  continuous. Nonetheless, the derivatives of the deformations  $i_{12}$ ,  $i_{13}$ , and  $i_{23}$  are the only ones appearing in the presented second gradient energy and, therefore, are the only ones on which the continuity has to be imposed.

### 3. Application cases

In the following subsection, two application cases proposed are presented: the first given by a material manufacturer, while the second by an end-user. Considering the two presented application cases, the prediction of the performance KPIs will be made through material modeling workflow (MODA), see [27], as the ones in Figure 1. The number and type of models could change depending on the scale of initial input (micro/meso/macro) and on the required detail (some properties can be assumed to shorten the process). A Multi-Physics Integration Platform (MuPIF) is used in this context to facilitate the implementation of multi-physics and multi-level simulations built from independently developed components, see [1, 28]. The

<sup>3</sup>[[ $\cdot$ ]] denotes the jump at the interface of the quantity.

main role of the platform will be to steer individual components (applications) and to provide high-level data exchange services. Each application will implement an interface that allows to steer application and execute data requests. The design supports various coupling strategies, discretization techniques, and also distributed applications. Furthermore, high performance materials design not only requires comprehensive material properties modeling but also understanding of risks, costs, and business opportunities for a range of decisions, from material selection to designing functional structural components and systems and process optimization.

#### 3.1. First use-case: thermoplastic airframe

The thermoplastic airframe is a suitable application case to evaluate the capabilities of the developed reduced order technology to provide with formability KPI. The object of our investigation is a thermoplastic fuselage frame made with a high strength carbon fiber system. The woven composite is made with 12 superposed plies of carbon for a total thickness of around 2.5mm and the simplified geometry presented in Figure 2. The rest of the technical data is confidential and is, therefore, not reported here.

#### 3.2. Second use-case: automotive leaf spring

The second application case concerns the material selection for a composite leaf spring at a conceptual design stage (Figure 3). Composite leaf springs serve as the elastic

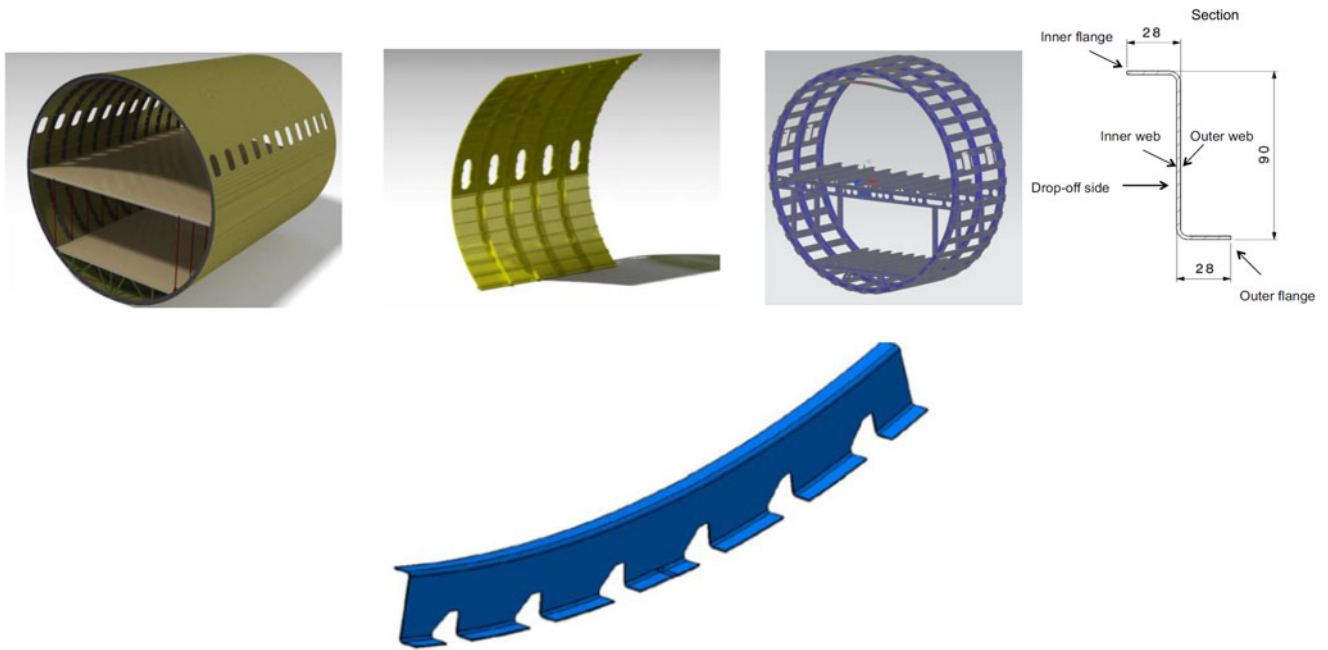


Figure 2. Geometry of the thermoplastic airframe application case.



Figure 3. Transverse Rear Leaf springs (top) and assumed geometry (bottom).

elements and guiding mechanism of the suspension in automotive design and are, therefore, some of the parts that need higher strength in the automobiles. Hence, static and dynamic mechanical properties, fatigue reliability and resistance to impact play a significant role in the material selection. In this application case, performance (stiffness, fatigue, damping), weight, time cycle, processing, material usage, cost, and recyclability are the KPIs.

The dimensions of the existing conventional middle leaf (spring) of a commercial vehicle were chosen for the design and manufacture of the die needed to mold the composite leaf-spring, see Figure 3. The cross sectional area of the leaf spring is 1.8cm thick and 7cm wide. Given the relevant thickness we will assume that a 2.5D woven composite is used, granting the integrity via a weave on the out-of-plane direction.

The simulation of the fiber reinforcement forming is necessary to simulate the impregnation process, giving fundamental data such as the local permeability and fiber direction, but also to give information on the final composite part. If the positioning and direction of fibers changes, both the directions and entity of maximum stiffness and strength will change drastically. Moreover, there is a threshold level of shear deformation before the reinforcement starts to dissociate, leading to a low quality of the final piece. For this reason, extensive studies regarding the modeling of raw fibrous composite materials can be found in the literature (e.g. [29–35]).

The difficulties to model the forming are due to local relative movements between the fibers that occur in dry composites. The resulting tensile stiffness of the homogenized material in the fiber direction is comparable to the

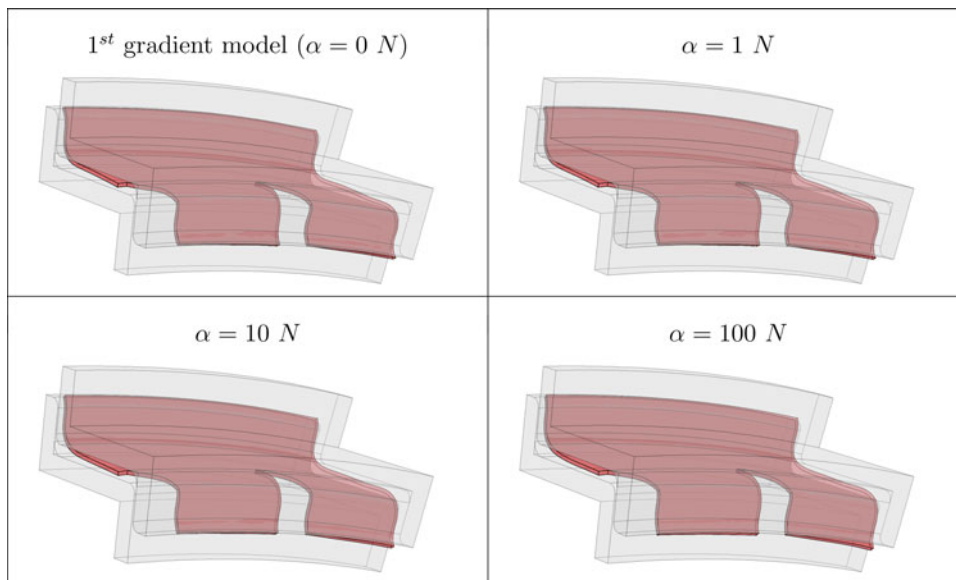


**Figure 4.** Case 1: dependence of the solution on the second gradient parameter  $\alpha$ .

stiffness of the material composing the fibers and, therefore, it is much larger than all the others rigidities (shear, bending, compaction). This quasi-inextensibility implies that the shear angle between warp and weft yarns can change without any relevant extension of the yarns. Furthermore, the coupling between the relatively low shear stiffness and the presence of slippages in the fabric makes it possible to have local bending of the yarns. The local curvature can significantly differ from the global one assumed by the whole piece, so giving a non-conventional influence to the local bending stiffness of the yarns with effects at the macroscopic level. Even considering the local slippages, fibrous composites can be (and generally are) considered continuous media with a reasonable accuracy. However, a classical model cannot account for phenomena related to the local bending stiffness of the yarns and it can mispredict the presence (or lack thereof) of defects in the material. On the other hand, a second gradient model can account directly for the curvature of the yarns at the mesoscopic level giving a more accurate description of the forming of dry fibrous composite reinforcements (see [6–11]).

## 4. Numerical results and effects of the second gradient parameter

### 4.1. Deformed shape

The model here presented implements the *augmented continuity shape functions* in a COMSOL<sup>®</sup> finite element model. The energy considered was the sum of the first gradient energy presented in Eq. (3) and of the second gradient one given in Eq. (5), for which the directions of the fibers  $D_1$  and  $D_2$  were chosen to be parallel to the edges of the specimen. The first gradient parameters are the ones shown in the Table 1, while various values of the second gradient parameter  $\alpha$  were considered. It must be noted that, in the case  $\alpha=0$ , the model reduces to a first gradient model with the energy of Eq. (3).

First, we analyze the thermoplastic airframe application case, whose slight double curvature and cut geometry give

rise to some additional transversal effects. The results, obtained for  $\alpha = 0, 1, 10, 100 N$ , are shown in Figure 4 for an imposed displacement of around 85% of the final one (30 cm). In contrast to the case of the deep drawing presented in [8], there is no significant wrinkling phenomenon both with and without the second gradient energy. Moreover, there is no significant influence of the second gradient parameter on the deformed shape either, leading to question the usefulness of a more complex model for this application case. Nonetheless, we will show in the following that the second gradient parameter has an influence on the deformation modes and it can be necessary to thoroughly describe the mechanical behavior of the woven composites. Even if it appears small, the effect could drastically change the results in terms of strain and porosity, leading to an accurate prediction of the curing process.

For the automotive leaf spring, there is some more visible difference between the displacements obtained for various second gradient parameters, see Figure 5. When the second gradient parameter increases, the central part of the specimen lifts and tends to have a constant curvature. As we will see in the following, a change in the deformation mode causes the difference in shape: a pure shear mode allows for higher curvatures than a constant curvature bending. As a matter of fact, this change reflects in the strain of the central part and proves how the deformation mode can be controlled and tuned with a second gradient model.

### 4.2. Deformation modes

A higher bending stiffness of the yarns changes the inner workings of the material in terms of deformation modes. Composite reinforcements have a very low shear stiffness, therefore the main deformation modes are the in-plane shear deformation, measured as  $i_{12} = D_1 \cdot C \cdot D_2$ , and the out-of-plane one, measured as  $i_{13} = D_1 \cdot C \cdot D_3$  and  $i_{23} = D_2 \cdot C \cdot D_3$ . The stiffness of the yarns in elongation, associated to the deformations  $i_{jj} = D_j \cdot C \cdot D_j$ , has a different

order of magnitude than the shear one, consequently the specimen tends to deform accordingly. For this reason, the chosen second gradient energy acts on the derivatives of the shear deformation to model the local bending stiffness of the yarns and to avoid unrealistic concentrations of shear deformation that would not be allowed by the micro-

structure of the woven composite. If this second gradient energy is high enough, the derivative of the shear (curvature of the yarn) is reduced spreading the effects of a concentrated external action. The usefulness of a second gradient energy is to control such effects with a limited set of parameters (only one with our assumptions). For very high

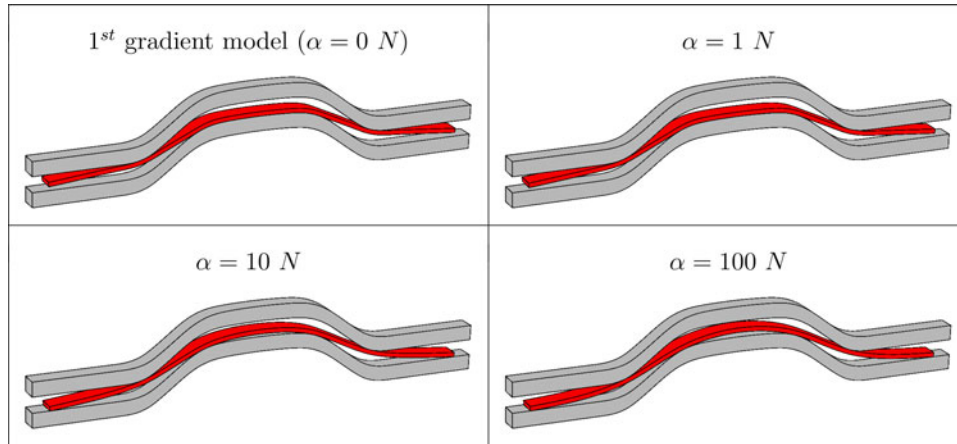


Figure 5. Case 2: dependence of the solution on the second gradient parameter  $\alpha$ .

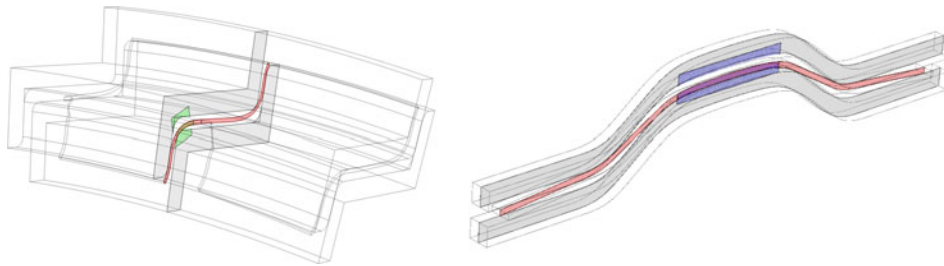


Figure 6. Cut planes for the analysis of the deformation modes (case 1 on the left and case 2 on the right). The green and blue areas will be used to show local effects.

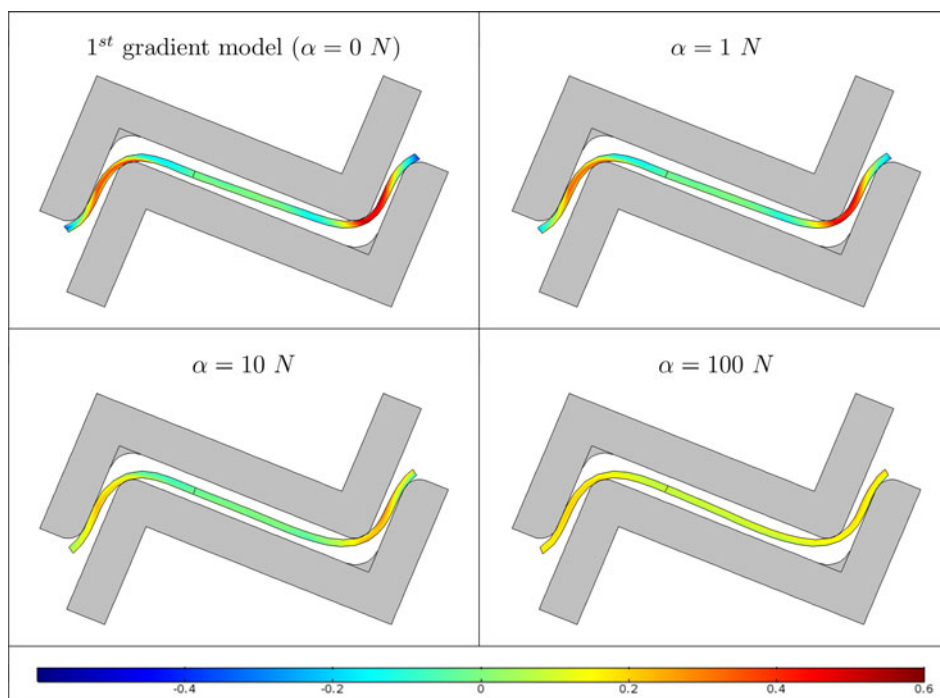


Figure 7. Case 1: dependence of the deformation  $i_{13}$  on the second gradient parameter  $\alpha$ .



bending stiffness (and second gradient parameter), the specimen assumes a constant minimum curvature that reduces the maximum value assumed by the shear deformation by spreading it on a larger area of the specimen.

To study these effects, we define one 2D cut-plane for each of the application cases on which we will plot the resulting strains, see Figure 6.

In the first application case, the increase of the second gradient parameter both decreases the shear deformation and distributes it, see Figure 7. We start by remarking that the results are not exactly symmetric due to the holes in the geometry (on the left in the cut-plane representation) but the behavior is still similar on the two sides of the specimen. The general qualitative behavior that we expected is confirmed:

- in the first gradient case, the shear deformation is substantial in the high-curvature-zones of the specimen and it decreases rapidly in the area near the contact points;

- increasing the second gradient parameter, the maximum value of the shear deformation drops and the area with relevant shear deformation around the contact point increases;
- when we reach the highest second gradient parameter considered, the shear deformation is spread on a relevant area reaching also the edges of the specimen, the maximum value of the shear deformation dropped to a fourth of the original one and the deformed shape has an almost constant small curvature on a relevant area around the contact points.

Also in the leaf spring case, the shear deformation decreases in maximum value and is redistributed in a larger area, see Figure 8: the deformation mode is of pure shear in the first gradient model, while increasing the second gradient parameter it becomes one of almost constant pure bending. Furthermore, the constant curvature is much more recognizable in this case due to the much simpler geometry. In the first gradient model, the geometry follows the mold

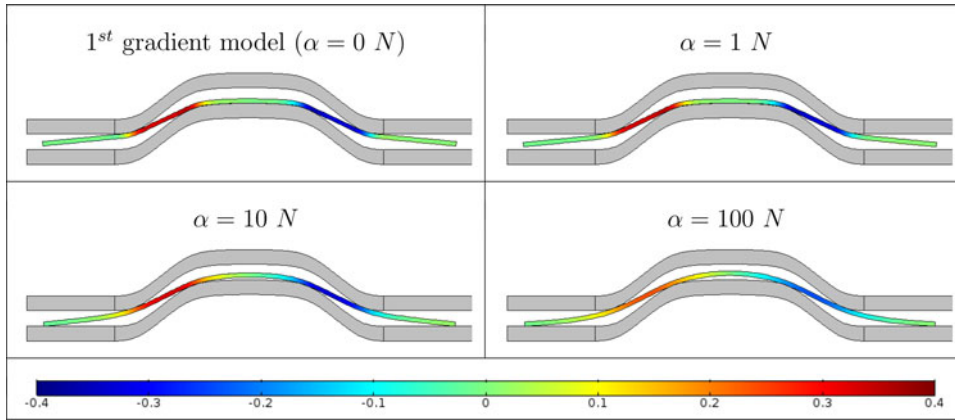


Figure 8. Case 2: dependence of the deformation  $i_{13}$  on the second gradient parameter  $\alpha$ .

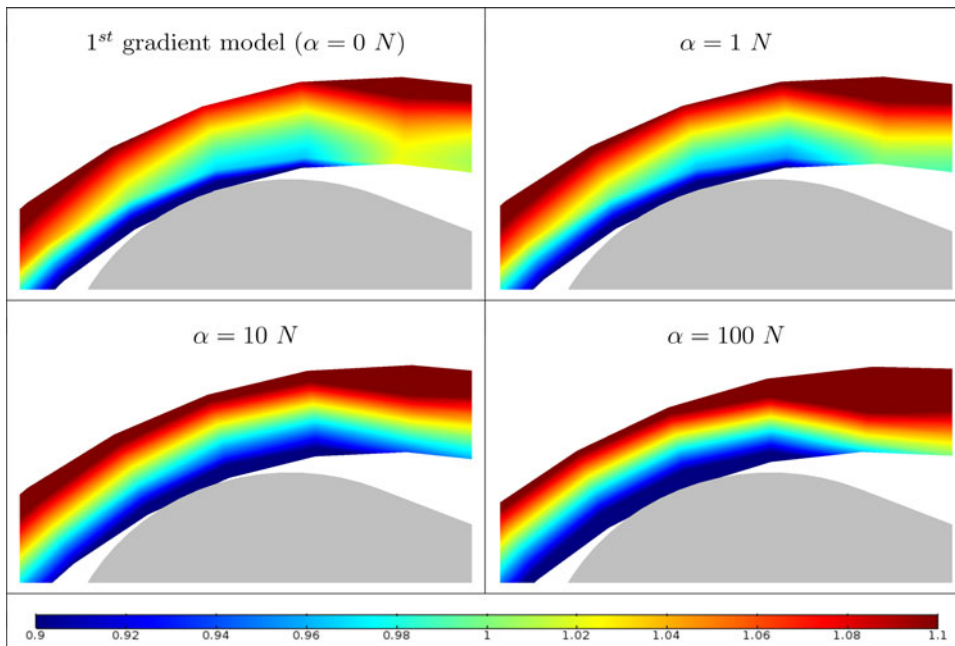


Figure 9. Case 1: dependence of the deformation  $i_{11}$  on the second gradient parameter  $\alpha$  (green area in Figure 6).

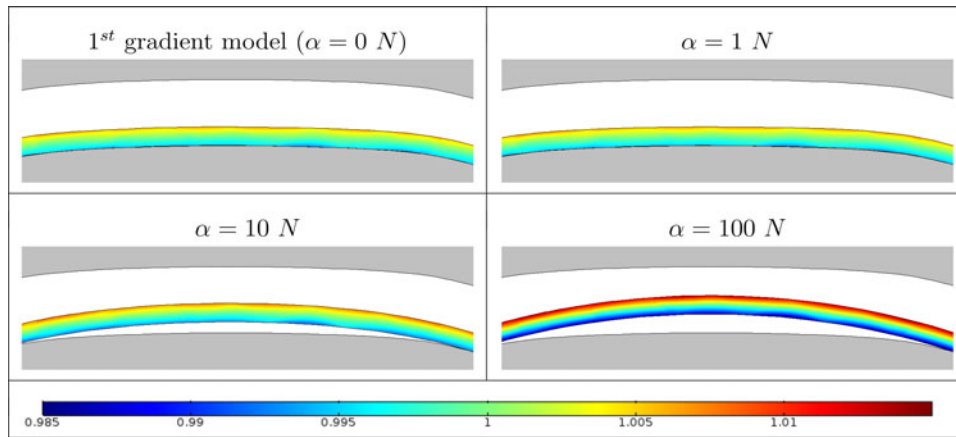


Figure 10. Case 2: dependence of the deformation  $i_{11}$  on the second gradient parameter  $\alpha$  (blue area in Figure 6).

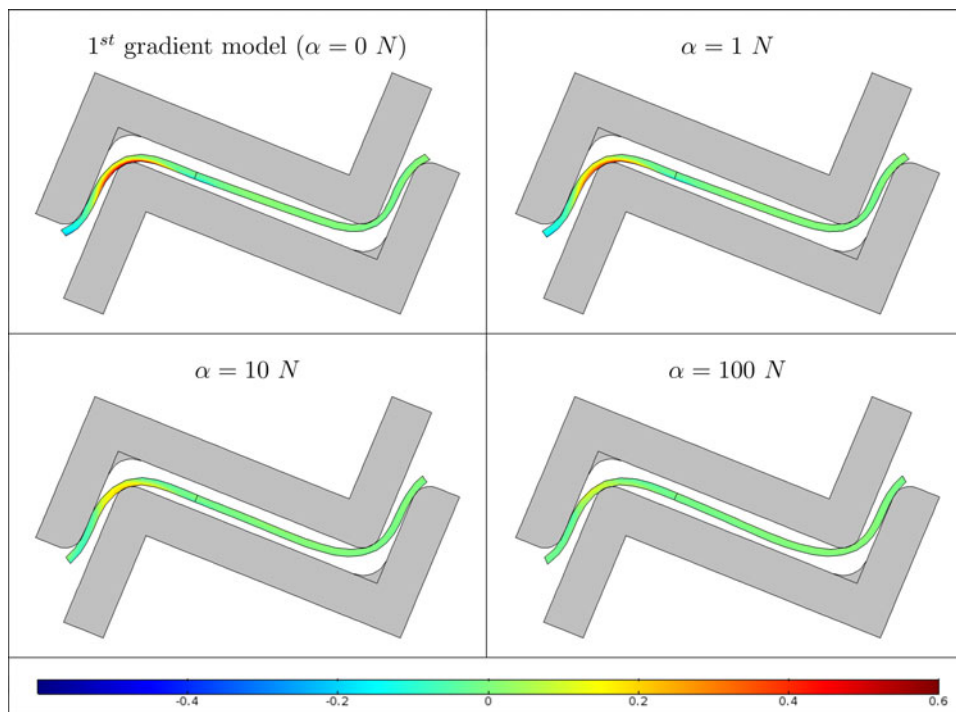


Figure 11. Case 1: dependence of the deformation  $i_{23}$  on the second gradient parameter  $\alpha$ .

even in the areas with relevant curvature. When we consider the limiting case of  $\alpha = 100N$ , the maximum curvature of the specimen is much lower than the one of the mold and the central part of the specimen lifts from the mold. Of course, the limiting case would happen only with extremely stiff yarns, but there are intermediate cases in which a small detachment could be observed experimentally.

The change in the shear distribution and magnitude leads to a classical bending deformation: the upper yarns tend to elongate while the lower yarns tend to compress. Therefore, penalizing the shear mode implies a reduction in shear deformation and also an increase in the extension of the yarns. To better show this behavior, we zoom in the area around the contact point of the thermoplastic airframe (green area in Figure 6) and we plot the elongation  $i_{11}$  of the yarns, see Figure 9. Due to the reduction of the shear, the specimen tends to behave more like an homogeneous

solid with a higher shear stiffness. Increasing the second gradient parameter, the upper yarns tend to elongate more with an increase of the compression of the lower yarns. This effect is due by the fictive increase of shear stiffness given by the spreading effect of the second gradient: penalizing the shear deformation, the elongation has to augment. Considering the second application case, in the central area of the specimen (blue area in Figure 6), the described effect on the deformation  $i_{11}$  is even more visible, see Figure 10. Here, we notice how the second gradient energy induces the constant curvature and the lift of the central part. Furthermore, the consequent increase on the elongation of the yarns is much more significant than the first case. When the second gradient parameter  $\alpha$  reaches the maximum value the constant-curvature-behavior is clearly visible and the upper part and lower part of the specimen have relevant and opposite elongational behaviors. This effect could be

used to tune the second gradient parameter with experimental results, since both the lift from the mold and the strains are observable quantities. Moreover, the proposed geometry has no relevant transverse effect, rendering the separate description of the effect of the two sets simpler.

Analyzing the thermoplastic airframe case, the area with most of the transverse effects is concentrated around the contact point, therefore we will plot the shear deformation  $i_{23}$  zooming in the relevant area, see Figure 11. Some possible remarks on the transverse shear deformation  $i_{23}$  are analogous to the longitudinal case:

- for the first gradient model, the value of the shear deformation around the contact point is very high;
- increasing the second gradient parameter the maximum value of the shear deformation drops.

However, there is one important difference to point out. The shear deformation decreases in magnitude but it is not spread more in the considered section. The reason for this effect is that the second gradient energy describes the bending stiffness of the yarns and, therefore, it spreads the shear deformation along the direction of the bent yarns. Having considered the transverse curvature, the redistribution of the shear will have to happen on the transverse direction, thus it will not be visible here. We refrain to show plots on the transverse direction since, the transverse curvature being constant, no interesting phenomena occur.

Since there is no transverse curvature in the leaf spring, there are no transverse effects and we will not show any transverse characteristics.

## 5. Conclusions

This paper shows how the use of a second gradient energy influences the deformation modes of a woven composite. In particular, two real geometries, taken from the COMPOSELECTOR project, are considered: an airframe for aeronautic industry and an automotive leaf spring used. The second gradient energy considered takes into account the in-plane and out-of-plane bending stiffness of the carbon yarns by means of a homogenized energy. The results are analyzed in terms of strains to show the influence of the second gradient parameter. Both examples show the same qualitative effects, the deformation mode switches from a shear one to one with a constant curvature along the specimen. This characteristic could be used to fit the proposed second gradient energy with real experiments, increasing the possibilities already provided in previous contributions (boundary layers, wrinkling, curvature of the boundary, etc.).

## Acknowledgments

The authors would like to acknowledge the support of EU H2020 COMPOSELECTOR project (Grant No: 721105).

## ORCID

Gabriele Barbagallo  <http://orcid.org/0000-0002-7047-7117>  
 Marco Valerio d'Agostino  <http://orcid.org/0000-0003-2966-1980>  
 Ali Daouadji  <http://orcid.org/0000-0003-1697-6465>  
 Ahmed Makradi  <http://orcid.org/0000-0003-1447-9713>  
 Gaetano Giunta  <http://orcid.org/0000-0003-1694-5132>  
 Philippe Boisse  <http://orcid.org/0000-0001-5930-3047>  
 Salim Belouettar  <http://orcid.org/0000-0002-2986-2902>  
 Angela Madeo  <http://orcid.org/0000-0003-1940-9853>

## References

- [1] S. Belouettar *et al.*, Integration of material and process modeling in a business decision support system: Case of composelector h2020 project, *Compos. Struct.*, vol. 204, pp. 778–790, 2018. DOI: [10.1016/j.compstruct.2018.06.121](https://doi.org/10.1016/j.compstruct.2018.06.121).
- [2] Q. Shao *et al.*, A data-driven analysis on bridging techniques for heterogeneous materials and structures, *Mech. Adv. Mater. Struct.*, pp. 1–15, 2019. DOI: [10.1080/15376494.2018.1546415](https://doi.org/10.1080/15376494.2018.1546415).
- [3] E. Laurini, D. Marson, M. Fermeglia, and S. Pricl, Multimodel approach for accurate determination of industry-driven properties for Polymer Nanocomposite Materials, *J. Comput. Sci.*, vol. 26, pp. 28–38, 2018. DOI: [10.1016/j.jocs.2018.03.002](https://doi.org/10.1016/j.jocs.2018.03.002). URL <http://linkinghub.elsevier.com/retrieve/pii/S1877750317312292>
- [4] P. Boisse, N. Hamila, and A. Madeo, The difficulties in modeling the mechanical behavior of textile composite reinforcements with standard continuum mechanics of Cauchy. Some possible remedies, *Int. J. Solids Struct.*, vol. 154, pp. 1–11, 2018. DOI: [10.1016/j.ijsolstr.2016.12.019](https://doi.org/10.1016/j.ijsolstr.2016.12.019).
- [5] A. Charmetant, J. G. Orliac, E. Vidal-Sallé, and P. Boisse, Hyperelastic model for large deformation analyses of 3D interlock composite preforms, *Compos. Sci. Technol.*, vol. 72, no. 12, pp. 1352–1360, 2012. DOI: [10.1016/j.compscitech.2012.05.006](https://doi.org/10.1016/j.compscitech.2012.05.006).
- [6] G. Barbagallo, Modeling fibrous composite reinforcements and metamaterials: Theoretical development and engineering applications, Ph.D. thesis, INSA–Lyon, 2017. DOI: [10.13140/RG.2.2.26062.56649](https://doi.org/10.13140/RG.2.2.26062.56649).
- [7] G. Barbagallo *et al.*, Bias extension test on an unbalanced woven composite reinforcement: Experiments and modeling via a second-gradient continuum approach, *J. Compos. Mater.*, vol. 51, no. 2, pp. 153–170, 2017. arXiv:1604.04298, DOI: [10.1177/0021998316643577](https://doi.org/10.1177/0021998316643577).
- [8] G. Barbagallo, A. Madeo, F. Morestin, and P. Boisse, Modelling the deep drawing of a 3D woven fabric with a second gradient model, *Math. Mech. Solids*, vol. 22, no. 11, pp. 2165–2179, 2017. DOI: [10.1177/1081286516663999](https://doi.org/10.1177/1081286516663999).
- [9] M. Ferretti, A. Madeo, F. dell'Isola, and P. Boisse, Modeling the onset of shear boundary layers in fibrous composite reinforcements by second-gradient theory, *Zeitschrift für Angewandte Mathematik und Physik*, vol. 65, no. 3, pp. 587–612, 2014. DOI: [10.1007/s00033-013-0347-8](https://doi.org/10.1007/s00033-013-0347-8).
- [10] A. Madeo, G. Barbagallo, M. V. d'Agostino, and P. Boisse, Continuum and discrete models for unbalanced woven fabrics, *Int. J. Solids Struct.*, vol. 94–95, pp. 263–284, 2016. DOI: [10.1016/j.ijsolstr.2016.02.005](https://doi.org/10.1016/j.ijsolstr.2016.02.005).
- [11] A. Madeo, M. Ferretti, F. dell'Isola, and P. Boisse, Thick fibrous composite reinforcements behave as special second-gradient materials: Three-point bending of 3D interlocks, *Zeitschrift für Angewandte Mathematik und Mechanik*, vol. 66, no. 4, pp. 2041–2060, 2015. DOI: [10.1007/s00033-015-0496-z](https://doi.org/10.1007/s00033-015-0496-z).
- [12] R. W. Ogden, *Non-Linear Elastic Deformations*, vol. 1. Mineola, NY: Dover Publications, Inc, 1984. DOI: [10.1016/0955-7997\(84\)90049-3](https://doi.org/10.1016/0955-7997(84)90049-3).
- [13] D. J. Steigmann, Invariants of the stretch tensors and their application to finite elasticity theory, *Math. Mech. Solids*, vol. 7, no. 4, pp. 393–404, 2002. DOI: [10.1177/108128028481](https://doi.org/10.1177/108128028481).

- [14] M. Itskov and N. Aksel, A class of orthotropic and transversely isotropic hyperelastic constitutive models based on a polyconvex strain energy function, *Int. J. Solids Struct.*, vol. 41, no. 14, pp. 3833–3848, 2004. DOI: [10.1016/j.ijsolstr.2004.02.027](https://doi.org/10.1016/j.ijsolstr.2004.02.027).
- [15] D. J. Steigmann, Frame-invariant polyconvex strain-energy functions for some anisotropic solids, *Math. Mech. Solids*, vol. 8, no. 5, pp. 497–506, 2003. DOI: [10.1017/CBO9781107415324.004](https://doi.org/10.1017/CBO9781107415324.004).
- [16] A. Raoult, Symmetry groups in nonlinear elasticity: An exercise in vintage mathematics, *Commun. Pure Appl. Anal.*, vol. 8, no. 1, pp. 435–456, 2008. DOI: [10.3934/cpaa.2009.8.435](https://doi.org/10.3934/cpaa.2009.8.435).
- [17] Y. Aimène, E. Vidal-Sallé, B. Hagège, F. Sidoroff, and P. Boisse, A hyperelastic approach for composite reinforcement large deformation analysis, *J. Compos. Mater.*, vol. 44, no. 1, pp. 5–26, 2010. DOI: [10.1177/0021998309345348](https://doi.org/10.1177/0021998309345348).
- [18] A. Charmetant, E. Vidal-Sallé, and P. Boisse, Hyperelastic modelling for mesoscopic analyses of composite reinforcements, *Compos. Sci. Technol.*, vol. 71, no. 14, pp. 1623–1631, 2011. DOI: [10.1016/j.compscitech.2011.07.004](https://doi.org/10.1016/j.compscitech.2011.07.004).
- [19] J.-J. Alibert, P. Seppecher, and F. dell’Isola, Truss modular beams with deformation energy depending on higher displacement gradients, *Math. Mech. Solids*, vol. 8, no. 1, pp. 51–73, 2003. DOI: [10.1177/1081286503008001658](https://doi.org/10.1177/1081286503008001658).
- [20] P. Seppecher, J.-J. Alibert, and F. dell’Isola, Linear elastic trusses leading to continua with exotic mechanical interactions, *J. Phys.: Conf. Series*, vol. 319, no. 1, 012018, 2011. DOI: [10.1088/1742-6596/319/1/012018](https://doi.org/10.1088/1742-6596/319/1/012018).
- [21] B. Nadler, P. Papadopoulos, and D. J. Steigmann, Multiscale constitutive modeling and numerical simulation of fabric material, *Int. J. Solids Struct.*, vol. 43, no. 2, pp. 206–221, 2006. DOI: [10.1016/j.ijsolstr.2005.05.020](https://doi.org/10.1016/j.ijsolstr.2005.05.020).
- [22] O. C. Zienkiewicz and R. L. Taylor, *The Finite Element Method Volume 1: The Basis*, 5th ed. Butterworth-Heinemann, Oxford, UK, 2000.
- [23] L. Greco and M. Cuomo, B-Spline interpolation of Kirchhoff-Love space rods, *Comput. Methods Appl. Mech. Eng.*, vol. 256, pp. 251–269, 2013. DOI: [10.1016/j.cma.2012.11.017](https://doi.org/10.1016/j.cma.2012.11.017).
- [24] L. Greco and M. Cuomo, An implicit G1 multi patch B-spline interpolation for Kirchhoff-Love space rod, *Comput. Methods Appl. Mech. Eng.*, vol. 269, pp. 173–197, 2014. DOI: [10.1016/j.cma.2013.09.018](https://doi.org/10.1016/j.cma.2013.09.018).
- [25] S. Zhang, A family of 3D continuously differentiable finite elements on tetrahedral grids, *Appl. Numer. Math.*, vol. 59, no. 1, pp. 219–233, 2009. DOI: [10.1016/j.apnum.2008.02.002](https://doi.org/10.1016/j.apnum.2008.02.002).
- [26] A. Ženišek, Polynomial approximation on tetrahedrons in the finite element method, *J. Approx. Theory*, vol. 7, no. 4, pp. 334–351, 1973. DOI: [10.1016/0021-9045\(73\)90036-1](https://doi.org/10.1016/0021-9045(73)90036-1).
- [27] A. F. de Baas, What Makes a Material Function? Let Me Compute the Ways... Modelling in H2020 LEIT-NMBP Programme Materials and Nanotechnology Projects. Luxembourg: Publications Office of the European Union, 2017. DOI: [10.2777/404734](https://doi.org/10.2777/404734).
- [28] B. Patzák, D. Rypl, and J. Kruijs, MuPIF-A distributed multi-physics integration tool, *Adv. Eng. Softw.*, vol. 60–61, pp. 89–97, 2013. DOI: [10.1016/j.advengsoft.2012.09.005](https://doi.org/10.1016/j.advengsoft.2012.09.005).
- [29] P. Boisse, K. Buet, A. Gasser, and J. Launay, Meso/macro-mechanical behaviour of textile reinforcements for thin composites, *Composites Sci. Technol.*, vol. 61, no. 3, pp. 395–401, 2001. DOI: [10.1016/S0266-3538\(00\)00096-8](https://doi.org/10.1016/S0266-3538(00)00096-8).
- [30] P. Boisse, N. Hamila, F. Helenon, B. Hagège, and J. Cao, Different approaches for woven composite reinforcement forming simulation, *Int. J. Mater. Form.*, vol. 1, no. 1, pp. 21–29, 2008. DOI: [10.1007/s12289-008-0002-7](https://doi.org/10.1007/s12289-008-0002-7).
- [31] P. Boisse, B. Zouari, and A. Gasser, A mesoscopic approach for the simulation of woven fibre composite forming, *Compos. Sci. Technol.*, vol. 65, no. 3–4, pp. 429–436, 2005. DOI: [10.1016/j.compscitech.2004.09.024](https://doi.org/10.1016/j.compscitech.2004.09.024).
- [32] E. de Luycker, F. Morestin, P. Boisse, and D. Marsal, Simulation of 3D interlock composite preforming, *Compos. Struct.*, vol. 88, no. 4, pp. 615–623, 2009. DOI: [10.1007/s12289-008-0267-x](https://doi.org/10.1007/s12289-008-0267-x).
- [33] E. de Luycker *et al.*, Experimental and numerical analyses of 3D interlock composite preforming, *Int. J. Mater. Form.*, vol. 3, no. S1, pp. 719–722, 2010. DOI: [10.1007/s12289-010-0871-4](https://doi.org/10.1007/s12289-010-0871-4).
- [34] S. Gatouillat, A. Bareggi, E. Vidal-Sallé, and P. Boisse, Meso modelling for composite preform shaping - Simulation of the loss of cohesion of the woven fibre network, *Compos. Part A: Appl. Sci. Manuf.*, vol. 54, pp. 135–144, 2013. DOI: [10.1016/j.compositesa.2013.07.010](https://doi.org/10.1016/j.compositesa.2013.07.010).
- [35] N. Hamila and P. Boisse, A meso-macro three node finite element for draping of textile composite preforms, *Appl. Compos. Mater.*, vol. 14, no. 4, pp. 235–250, 2007. DOI: [10.1007/s10443-007-9043-1](https://doi.org/10.1007/s10443-007-9043-1).
- [36] G. A. Holzapfel, T. C. Gasser, and R. W. Ogden, A new constitutive framework for arterial wall mechanics and a comparative study of material models, *J. Elasticity*, vol. 61, no. 1/3, pp. 1–48, 2000. DOI: [10.1023/A:1010835316564](https://doi.org/10.1023/A:1010835316564).
- [37] A. J. M. Spencer, “Constitutive theory for strongly anisotropic solids,” in *Continuum Theory of the Mechanics of Fibre-Reinforced Composites*, A. J. M. Spencer (Ed.). Vienna: Springer-Verlag, 1984, pp. 1–32. DOI: [10.1007/978-3-7091-4336-0](https://doi.org/10.1007/978-3-7091-4336-0).
- [38] R. W. Ogden, “Nonlinear elasticity, anisotropy, material stability and residual stresses in soft tissue,” in *Biomechanics of Soft Tissue in Cardiovascular Systems*, vol. 108. Vienna: Springer-Verlag, 2003, pp. 65–108. DOI: [10.1007/978-3-7091-2736-0\\_3](https://doi.org/10.1007/978-3-7091-2736-0_3).

## Appendix A: A representation theorems for hyperelastic materials

The main issue when defining a constitutive law is the choice of the deformation descriptors. In the literature, we find different theorems that ensure the minimum number of parameters needed to correctly represent the functional dependence of  $W$  on  $C$ . All of these results define a minimum number of invariants for any specific symmetry in the considered medium. For what follows the unitary vector along the preferred directions, namely the fiber directions in the case of the fabrics, will be denoted by  $m_1$  and  $m_2$  and the unitary vector  $m_3$  is defined as  $m_3 := m_1 \times m_2$ . The invariants considered in the following and a brief description of their meaning are listed in Table A1.

Considering an isotropic symmetry, various hyperelastic constitutive energy densities, which are suitable to describe the mechanical behavior even at finite strains, have been proposed in the literature (see e.g. [12, 13]). For orthotropic materials, constitutive hyperelastic equations are harder to be found in the literature. Plenty of authors try to generalize the representation theorems valid for isotropic and transversely isotropic media, but often there is no apparent agreement between the different proposed versions.

The most diffused version of the representation theorem for orthotropic materials (see e.g. [36–38]) states that only seven independent scalar invariants of the Cauchy-Green tensor  $C$  are sufficient to correctly represent the functional dependence of  $W^{orth}$  on  $C$ . In other words, for an orthotropic material, it is sufficient to consider an energy such as:

**Table A1.** Invariants of deformation.

Invariant	Expression	Meaning in terms of deformation
$i_1$	$\text{tr}(C)$	Changes of length
$i_2$	$\text{tr}(\det(C)C^{-T})$	Changes of area
$i_3$	$\det(C)$	Changes of volume
$i_4 = i_{11}$	$m_1 \cdot C \cdot m_1$	Local stretch in the direction $m_1$
$i_5$	$m_1 \cdot C^2 \cdot m_1$	Shear and stretch strain in $m_1$
$i_6 = i_{22}$	$m_2 \cdot C \cdot m_2$	Local stretch in the direction $m_2$
$i_7$	$m_2 \cdot C^2 \cdot m_2$	Shear and stretch strain in $m_2$
$i_8 = i_{12}$	$m_1 \cdot C \cdot m_2$	Shear strain between the directions $(m_1, m_2)$
$i_9 = i_{13}$	$m_1 \cdot C \cdot m_3$	Shear strain between the directions $(m_1, m_3)$
$i_{10} = i_{23}$	$m_2 \cdot C \cdot m_3$	Shear strain between the directions $(m_2, m_3)$
$i_{11}^* = i_{33}$	$m_3 \cdot C \cdot m_3$	Local stretch in the direction $m_3$

$$W^{orth}(C) = W(i_1, i_2, i_3, i_4, i_5, i_6, i_7) \quad (A1)$$

Nevertheless, only six independent scalar invariants are sufficient to completely describe the behavior of an orthotropic material (see the elegant proof given in [16]), so that, even if seven scalar invariants are considered, not all of them are truly independent functions of  $C$ . In particular, we

introduce the set of six invariants  $i_O := \{i_{11}, i_{22}, i_{33}, i_{12}, i_{13}, i_{23}\}$  to represent the functional dependence of  $W$  on  $C$ :

$$W^{orth}(C) = W(i_{11}, i_{22}, i_{33}, i_{12}, i_{13}, i_{23}) \quad (A2)$$

Indeed, all the other invariants can be expressed in terms of such six.